Title
Visualizing Heavy Fermion Formation and their Unconventional Superconductivity in f-Electron Materials

Journal
Journal of the Physical Society of Japan, 83(6)

ISSN
0031-9015

Authors
Aynajian, Pegor
da Silva Neto, Eduardo H
Zhou, Brian B
et al.

Publication Date
2014-06-15

DOI
10.7566/jpsj.83.061008

Journal of the Physical Society of Japan **83**, 061008 (2014)
http://dx.doi.org/10.7566/JPSJ.83.061008

Visualizing Heavy Fermion Formation and their Unconventional Superconductivity in *f*-Electron Materials

Pegor Aynajian[1*], Eduardo H. da Silva Neto[1†], Brian B. Zhou[1], Shashank Misra[1], Ryan E. Baumbach[2], Zachary Fisk[3], John Mydosh[4], Joe D. Thompson[2], Eric D. Bauer[2], and Ali Yazdani[1‡]

[1]*Joseph Henry Laboratories and Department of Physics, Princeton University, Princeton, NJ 08544, U.S.A.*
[2]*Los Alamos National Laboratory, Los Alamos, NM 87545, U.S.A.*
[3]*University of California, Irvine, CA 92697, U.S.A.*
[4]*Kamerlingh Onnes Laboratory, Leiden University, 2300 RA Leiden, The Netherlands*

(Received September 25, 2013; accepted November 14, 2013; published online May 9, 2014)

In solids containing elements with *f*-orbitals, the interaction between *f*-electron spins and those of itinerant electrons leads to the development of low-energy fermionic excitations with a heavy effective mass. These excitations are fundamental to the appearance of unconventional superconductivity observed in actinide- and lanthanide-based compounds. We use spectroscopic mapping with the scanning tunneling microscope to detect the emergence of heavy excitations with lowering of temperature in Ce- and U-based heavy fermion compounds. We demonstrate the sensitivity of the tunneling process to the composite nature of these heavy quasiparticles, which arises from quantum entanglement of itinerant conduction and *f*-electrons. Scattering and interference of the composite quasiparticles is used in the Ce-based compounds to resolve their energy-momentum structure and to extract their mass enhancement, which develops with decreasing temperature. Finally, by extending these techniques to much lower temperatures, we investigate how superconductivity, with a nodal *d*-wave character, develops within a strongly correlated band of composite excitations.

1. Introduction

A remarkable variety of collective electronic phenomena have been discovered in compounds with partially filled *f*-orbitals where electronic correlations are dramatically enhanced.[1,2)] In these compounds the entanglement of the rather localized *f*-electrons with the surrounding itinerant electrons starts at relatively high temperature leading to the development of low-energy composite quasiparticles with a heavy effective mass. Tuning the hybridization between *f*-orbitals and itinerant electrons can destabilize the heavy Fermi liquid state at low temperatures towards an antiferromagnetically ordered ground state.[3–8)] In proximity to such a quantum phase transition, between itinerancy and localization of *f*-electrons, many heavy fermion systems exhibit magnetism and unconventional superconductivity at low temperatures [Fig. 1(a)].[9)]

Thermodynamic and transport studies have long provided evidence for heavy quasiparticles, their unconventional superconductivity, and non-Fermi liquid behavior in a variety of Kondo lattice systems.[1,2,9–12)] However, the emergence of a coherent band of heavy quasiparticles near the Fermi energy, as a result of the hybridization of the localized *f*-electrons with conduction electrons [Fig. 1(b)], remains not well understood.[12–15)] Part of the challenge has been the inability of spectroscopic measurements to probe the development of heavy quasiparticles with lowering of temperature and to characterize their properties with high-energy resolution. Recently, various theoretical approaches, including several numerical studies, remarkably reproduce the generic composite band structure of Fig. 1(b).[16–20)] Theoretical modeling has also shown that tunneling spectroscopy can be a powerful probe of this composite nature of heavy fermions.[21–24)] Depending on the relative tunneling amplitudes to the light conduction (t_c) or to the heavy *f*-like (t_f) components of the composite quasiparticles, and due to their interference, tunneling spectroscopy can be sensitive to different features of the hybridized band structure [Figs. 1(c) and 1(d); see detail below]. Such precise measurements of heavy fermion formation are not only required for understanding the nature of these electronic excitations close to quantum phase transitions[25)] but are critical to identifying the source of unconventional superconductivity near such transitions, which continues to be at the forefront of unsolved problems in all of physics.

Here we review our recent advances in the application of STM techniques to study the formation of heavy fermions and their superconductivity.[26–28)] To provide a controlled study of the formation of heavy fermion excitations within a Kondo lattice system and visualize the emergence of heavy electron superconductivity, we carried out studies on the $Ce_1M_1In_5$ (with M = Co, Rh) material system. These so-called 115 compounds offer the possibility to tune the interaction between the Ce's *f*-orbitals and the itinerant *spd* conduction electrons using isovalent substitutions at the transition metal site within the same tetragonal crystal structure. Consequently, the ground state of this system can be tuned (in stoichiometric compounds) between antiferromagnetism, as in $CeRhIn_5$ ($T_N = 3.5\,K$), to superconductivity, as observed in $CeCoIn_5$ ($T_c = 2.3\,K$) and $CeIrIn_5$ ($T_c = 0.4\,K$).[9)] Transport studies show a drop in the electrical resistivity in $CeCoIn_5$ around $T^* = 50\,K$, which has been interpreted as evidence for the development of a coherent heavy quasiparticle band, followed by a linear resistivity at lower temperature (above T_c)[29)]—a behavior that has been associated with the proximity to the QCP. Quantum oscillations and thermodynamic measurements find a heavy effective mass (10–50m_0, where m_0 is the bare electron mass) for $CeCoIn_5$, while in the same temperature range the *f*-electrons in $CeRhIn_5$ are effectively decoupled from the conduction electrons.[30,31)]

We demonstrate the sensitivity of the tunneling process to the composite nature of these heavy quasiparticles in $CeCoIn_5$, which arises from quantum entanglement of itinerant conduction and *f*-electrons. We contrast this observation in $CeCoIn_5$ with the exotic heavy fermion

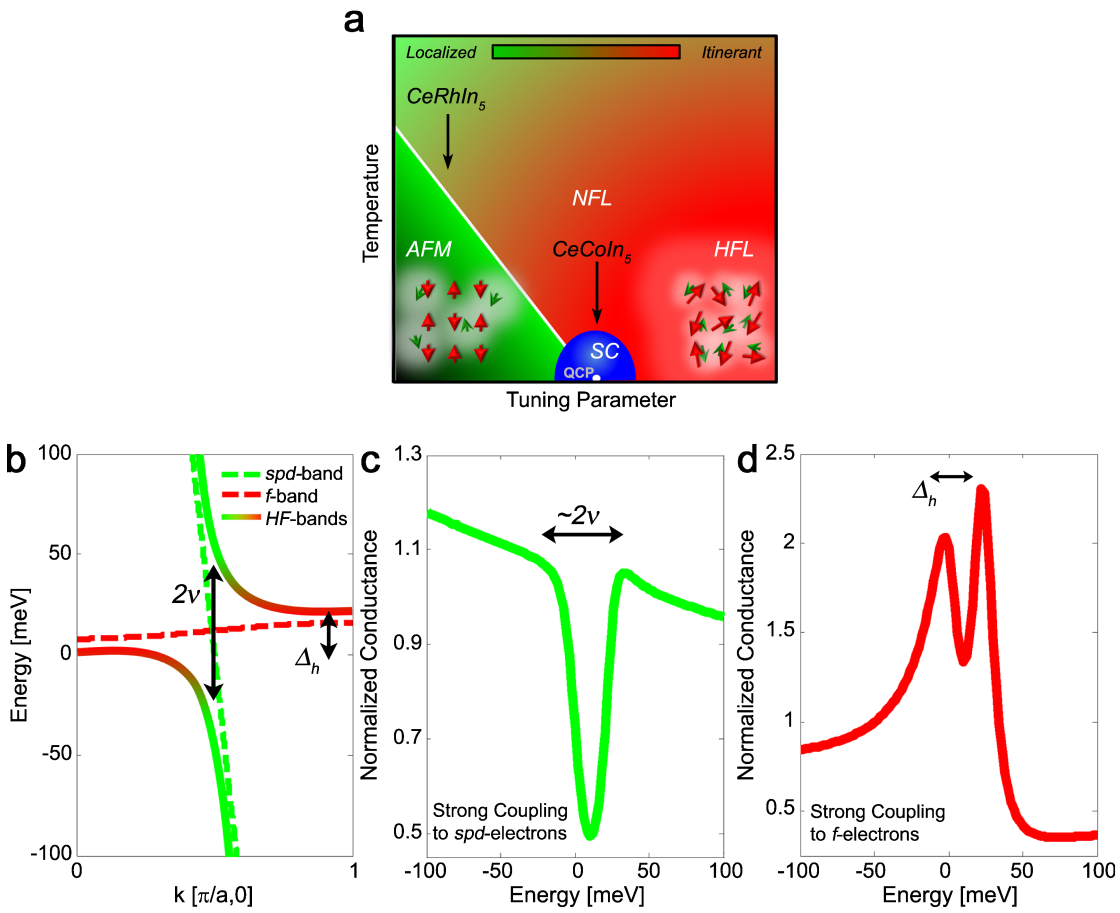

Fig. 1. (Color online) Tunneling into a Kondo lattice. (a) Schematic phase diagram of heavy-fermion systems where the electronic ground state can be tuned from antiferromagnetism (AFM) with localized *f*-moments to a heavy Fermi liquid (HFL) with itinerant *f*-electrons. At low temperatures, superconductivity (SC) sets in near the quantum critical point (QCP) from a non-Fermi liquid (NFL). (b) Bare electronic bands (dashed lines) and hybridized heavy fermion bands (HF) (solid lines) displaying a direct ($2v$) and an indirect (Δ_h) hybridization gaps. (c) Tunneling spectra computed from the hybridized band structure in (b) for a tunneling ratio $t_f/t_c = -0.025$ showing sensitivity to the direct hybridization gap ($2v$). (d) Similar spectra computed with $t_f/t_c = -0.37$ showing sensitivity to the indirect gap (Δ_h). Figure partially reproduced from Ref. 27.

compound URu_2Si_2, which also shows similar composite heavy fermion behavior at high temperatures but undergoes an enigmatic second order phase transition at $T_{HO} = 17.5\,K$ to a "hidden order" state. Using spectroscopic imaging of quasiparticle interference in Ce-115 compounds, we visualize the energy-momentum structure of these composite heavy fermion excitations which develops below T^* near the Fermi energy. Upon further lowering of temperature, we find the spectrum of these heavy excitations to be strongly modified just prior to the onset of superconductivity by a suppression of the spectral weight near E_F, reminiscent of the pseudogap state in the cuprates.[32,33] Finally, we demonstrate how nodal superconductivity develops within this strongly correlated band of composite excitations.

2. Experimental Results

2.1 Cleaved surfaces and topographs of $CeCoIn_5$

Figures 2(a) and 2(b) show STM topographs of a single crystal of $CeCoIn_5$ doped with 0.15% of Hg–CeCo-$(In_{0.9985}Hg_{0.0015})_5$ for reasons which will be addressed below. All high temperature measurements ($T \geq 20\,K$) were performed on $CeCo(In_{0.9985}Hg_{0.0015})_5$. For simplicity however, from here on we will refer to it as $CeCoIn_5$. The samples were cleaved in situ in our variable temperature ultra-high vacuum STM. The cleaving process results in exposing multiple surfaces terminated with different chemical compositions. The crystal symmetry necessarily requires multiple surfaces for cleaved samples, as no two equivalent consecutive layers occur within the unit cell. Therefore breaking of any single chemical bond will result in different layer terminations on the two sides of the cleaved sample. Experiments on multiple cleaved samples have mostly revealed three different surfaces, two of which are atomically ordered (termed surfaces A and B in Fig. 2) with a periodicity corresponding to the lattice constant of the bulk crystal structure, while the third surface (termed surface C, Fig. 2) is reconstructed. Comparison of the relative heights of the sub-unit cell steps between the different layers [Figs. 2(c) and 2(d)] to the crystal structure determined from scattering experiments[34] enables us to identify the chemical composition of each exposed surface [Fig. 2(d)]. Experiments on the isostructural $CeRhIn_5$ reveal similar results (not shown here), where cleaving exposes the corresponding multiple layers.

2.2 Composite nature of heavy fermion excitations in $CeCoIn_5$

Spectroscopic measurements of $CeCoIn_5$ show the sensitivity of the tunneling process to the composite nature of the hybridized heavy fermion states. As shown in Fig. 3(a), tunneling spectra on surface A (identified as the Ce–In layer)

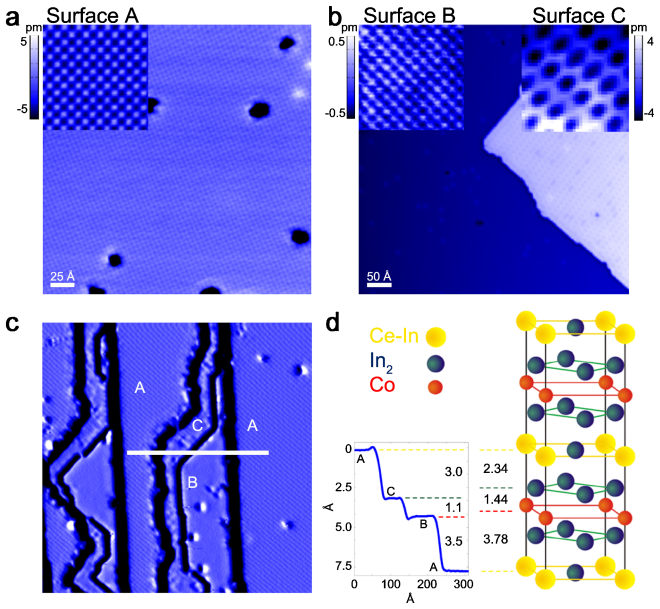

Fig. 2. (Color online) STM topographies on $CeCoIn_5$. (a) Constant current topographic image (+200 mV, 200 pA) showing an atomically ordered surface (termed surface A) with a lattice constant of ~4.6 Å. (b) Topographic image (−200 mV, 200 pA) showing two consecutive layers: a distinct atomically ordered surface (termed surface B, lattice constant ~4.6 Å) and a reconstructed surface (termed surface C). (c) Constant current topographic image (−150 mV, 365 pA) displaying all three surfaces (the derivative of the topography is shown to enhance contrast). (d) A line cut through the different surfaces (solid line in c) showing the relative step heights compared to the bulk crystal structure. Insets in (a) and (b) show blow-ups (45 × 45 $Å^2$) of the three different surfaces. Figure reproduced from Ref. 27.

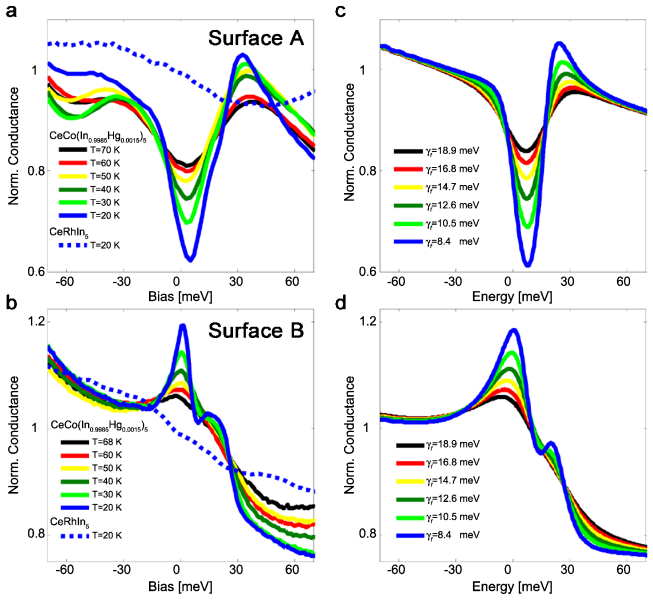

Fig. 3. (Color online) Composite nature of heavy fermion excitations in $CeCo(In_{0.9985}Hg_{0.0015})_5$. (a) Averaged tunneling spectra (−150 mV, 200 pA) measured on surface A of $CeCo(In_{0.9985}Hg_{0.0015})_5$ for different temperatures (solid lines) and on the corresponding surface A of $CeRhIn_5$ at 20 K (dashed line). Note that the CeCoIn5 sample was doped by 0.15% Hg, which does not affect the electronic properties. (b) Averaged tunneling spectra (−150 mV, 200 pA) measured on surface B of $CeCo(In_{0.9985}Hg_{0.0015})_5$ for different temperatures (solid lines) and on corresponding surface B of $CeRhIn_5$ at 20 K (dashed line). (c, d) Tunneling spectra computed for $t_f/t_c = -0.01$ (c) and $t_f/t_c = -0.20$ (d) for selected values of the f-component lifetime broadening γ_f. Figure reproduced from Ref. 27.

of $CeCoIn_5$ show that upon cooling the sample, dramatic changes develop in the spectra in an asymmetric fashion about the Fermi energy. The redistribution of the spectra observed on this surface is consistent with a tunneling process that is dominated by coupling to the light conduction electrons and displays signatures of the direct hybridization gap ($2v \approx 30$–40 meV) experienced by this component of the heavy fermion excitations [e.g., see Figs. 1(b) and 1(c)]. In contrast to these observations, similar measurements on the corresponding surface of $CeRhIn_5$ show spectra that are featureless in the same temperature range [Fig. 3(a), dashed line] and are consistent with the more localized nature of the Ce f-orbitals in $CeRhIn_5$ as compared to $CeCoIn_5$.

The composite nature of the heavy fermion excitations manifests itself by displaying different spectroscopic characteristics for tunneling into the different atomic layers. Figure 3(b) shows spectra measured on surface B (identified as Co) of $CeCoIn_5$ that looks remarkably different than those measured on surface A [Fig. 3(a)]. In the same temperature range where spectra on surface A [Fig. 3(a)] develop a depletion of spectral weight near the Fermi energy, surface B shows a sharp enhancement of spectral weight within the same 30–40 meV energy window [Fig. 3(b)]. With further lowering of temperature, the enhanced tunneling on surface B evolves into a double-peak structure. As a control experiment, measurements on the corresponding surface in $CeRhIn_5$, once again, display no sharp features in the same temperature and energy windows [Fig. 3(b), dashed line]. The spectroscopic features of $CeCoIn_5$'s surface B display the characteristic signatures of dominant tunneling to the f-component of the heavy quasiparticles, which reside near the Fermi energy and are expected to display the indirect hybridization gap (Δ_h) [see Figs. 1(b) and 1(d)].

A model calculation for tunneling to composite heavy excitations can reproduce the different spectroscopic lineshapes on the two different surfaces. Following recent theoretical efforts,[22,23] we compute the spectroscopic properties of a model band structure in which a single hole-like itinerant band of spd-like electrons $E_k^c(k_x, k_y)$ hybridizes with a narrow band of f-like electrons $E_k^f(k_x, k_y)$, with

$$E_k^c = 2t(\cos k_x + \cos k_y) - \mu,$$

$$E_k^f = -2\chi_0(\cos k_x + \cos k_y) - 4\chi_1 \cos k_x \cos k_y + \varepsilon_0^f.$$

Here, t and μ represent the nearest neighbor hopping of the conduction electrons and the chemical potential, respectively, and χ_0, χ_1, and ε_0^f represent the nearest and next-nearest site spin correlations, and the position of the heavy band with respect to the Fermi energy, respectively. The hybridization of these two bands with a hybridization amplitude v yields the generic heavy fermion band structure of Fig. 1(b). The differential conductance dI/dV, which represents the tunneling to the hybridized band structure, can then be calculated by

$$\frac{dI(k,\omega)}{dV} \propto -\frac{2e}{\hbar}\sum_{i,j=1}^{2}[\hat{t}\,\mathrm{Im}\,\hat{G}(k,\omega)\hat{t}]_{ij}.$$

Where the matrix $\hat{t}(t_c, t_f)$ controls the ratio of tunneling to the c- and f-bands and $\hat{G}$ defines the full Green's function describing the hybridization between the c- and f-electron bands.[22,23] The results of our calculations [Figs. 3(c) and

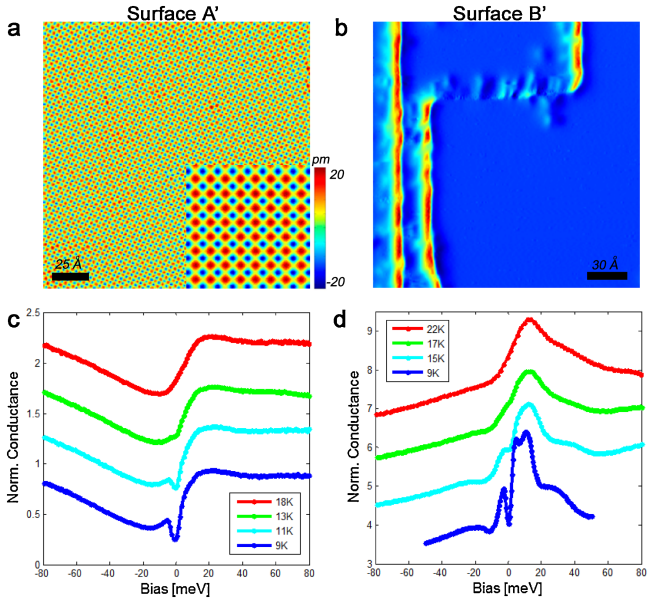

Fig. 4. (Color online) Heavy fermion excitations in URu_2Si_2. (a) Constant current topographic image (+200 mV, 60 pA) showing an atomically ordered surface (termed surface A′) with a lattice constant of ≈4.1 Å. (b) Topographic image (−200 mV, 200 pA) displayed in derivative mode showing a different cleaved surface (with single unit cell atomic steps) with much weaker atomic corrugations (termed surface B′). Note that this terminology is different than Ref. 26. (c) Averaged tunneling spectra (−200 mV, 200 pA) measured on surface A of URu_2Si_2 for different temperatures. (d) Similar spectra (−200 mV, 200 pA) measured on surface B showing the double peak structure at around 10 and 30 meV. On both surfaces, below the hidden order transition a gap opens near the Fermi energy. The spectra are offset for clarity. Panels a and c reproduced from Ref. 26.

3(d)] are strongly sensitive to the ratio of tunneling into the heavy *f*-states versus the light conduction band (t_f/t_c)—a behavior that explains the differences between the tunneling processes on the different cleaved surfaces [Figs. 3(a) and 3(b)]. Our calculations also capture the temperature evolution of the spectra in Fig. 3(b), by varying the inverse lifetime (scattering rate) of the *f*-component of the heavy quasiparticles in our model calculations [Fig. 3(d)]. These measurements and their corresponding modeling demonstrate the composite nature of heavy fermions excitations in $CeCoIn_5$.

2.3 *Heavy fermion formation in URu_2Si_2*

To demonstrate the generic behavior of the tunneling sensitivity to the composite nature of heavy fermion excitations, we show in Fig. 4 similar measurements carried out on another heavy fermion compound. URu_2Si_2 displays heavy electron formation below $T^* \approx 80$ K, as probed by transport measurements.[35] However, this compound has long puzzled scientists due to its enigmatic phase transition to a hidden order state at $T_{HO} = 17.5$ K, whose order parameter and connection to the heavy excitations has since remained a mystery.[10,36] In Figs. 4(a) and 4(b) we show STM topographs of the cleaved surfaces of URu_2Si_2, which similar to $CeCoIn_5$ expose multiple atomic layers within the unit cell. (Here we show the two relevant surfaces, A′ and B′. A third surface, which undergoes surface reconstruction, is also observed.[26] The terminology here is different than that in Ref. 26.) Spectroscopic measurements on the corresponding multiple surfaces of URu_2Si_2 at temperatures above T_{HO} [Figs. 4(c) and 4(d)] reveal different spectroscopic lineshapes, yet with notable similarities to those observed in $CeCoIn_5$ [Figs. 3(a) and 3(b)]. The spectra on surface A′ of URu_2Si_2 display an asymmetric Fano lineshape, a signature of quantum interference between tunneling to a discrete (t_f) and continuum (t_c) electronic states.[37,38] Similar measurements on surface B′ display a double peak structure, indicating an enhanced co-tunneling to the discrete *f*-like states on this surface. As in $CeCoIn_5$, the double-peak structure, extended over ≈40 meV, reflects the high density of states originating from the flat dispersions of the two heavy fermion bands [Figs. 1(b) and 1(d)], which are already formed above T_{HO}. These similarities in the two, rather different, material systems demonstrate the generic behavior of the tunneling process to the composite nature of heavy fermion excitations. Extending the measurements in URu_2Si_2 below T_{HO} further reveals that the hidden order occurs on the lower heavy fermion band with an energy scale of ≈4 meV around the Fermi energy—an order of magnitude smaller than the hybridization energy scale of ≈40 meV.

2.4 *Visualizing quasiparticle mass enhancement in $CeCoIn_5$*

To directly probe the energy-momentum structure of heavy quasiparticles we consider the Ce-115 material systems again. Spectroscopic mapping with the STM enables us to visualize scattering and interference of these quasiparticle excitations from impurities or structural defects. Elastic scattering of quasiparticles from these imperfections gives rise to standing waves in the conductance maps at wavelengths corresponding to $2\pi/q$, where $\boldsymbol{q} = \boldsymbol{k}_f - \boldsymbol{k}_i$ is the momentum transfer between initial ($\boldsymbol{k}_i$) and final ($\boldsymbol{k}_f$) states at the same energy. We expect that $\boldsymbol{q}$'s with the strongest intensity connect regions of high density of states on the contours of constant energy and hence provide energy-momentum information of the quasiparticle excitations. We characterize the scattering $\boldsymbol{q}$'s using discrete Fourier transforms (DFTs) of STM conductance maps measured at different energies. Figure 5(a) shows examples of energy-resolved STM conductance maps on surface A of $CeCoIn_5$ measured at 20 K displaying signatures of scattering and interference of quasiparticles from defects and step edges. These conductance maps show clear changes of the wavelength of the modulations as a function of energy. Perhaps the most noticeable are the changes around each random defect (0.15% of Hg dopants, which is doped intentionally to introduce quasiparticle scattering centers. Their presence, however, at this low concentration does not change the thermodynamic properties). Figure 5(b) shows DFTs of such maps that display sharp non-dispersive Bragg peaks [at the corners, $(\pm 2\pi/a, 0)$, $(0, \pm 2\pi/a)$] corresponding to the atomic lattice, as well as other features (concentric square-like shapes) that disperse with energy, collapse [Fig. 5(b); 0 meV], and disappear [Fig. 5(b); 9 meV] near the Fermi energy. We have carried out such measurements both at low temperatures [20 K, Fig. 5(b)], where the spectrum shows signatures of hybridization between conduction electrons and *f*-orbitals, as well as at high temperatures [70 K, Fig. 5(c)] where such features are considerably weakened [e.g., Fig. 5(c); 2 meV, 10 meV]. As a control experiment, we have also carried out the same measurements on the corresponding surface of $CeRhIn_5$ [Fig. 5(d)], for which signatures of heavy electron behavior

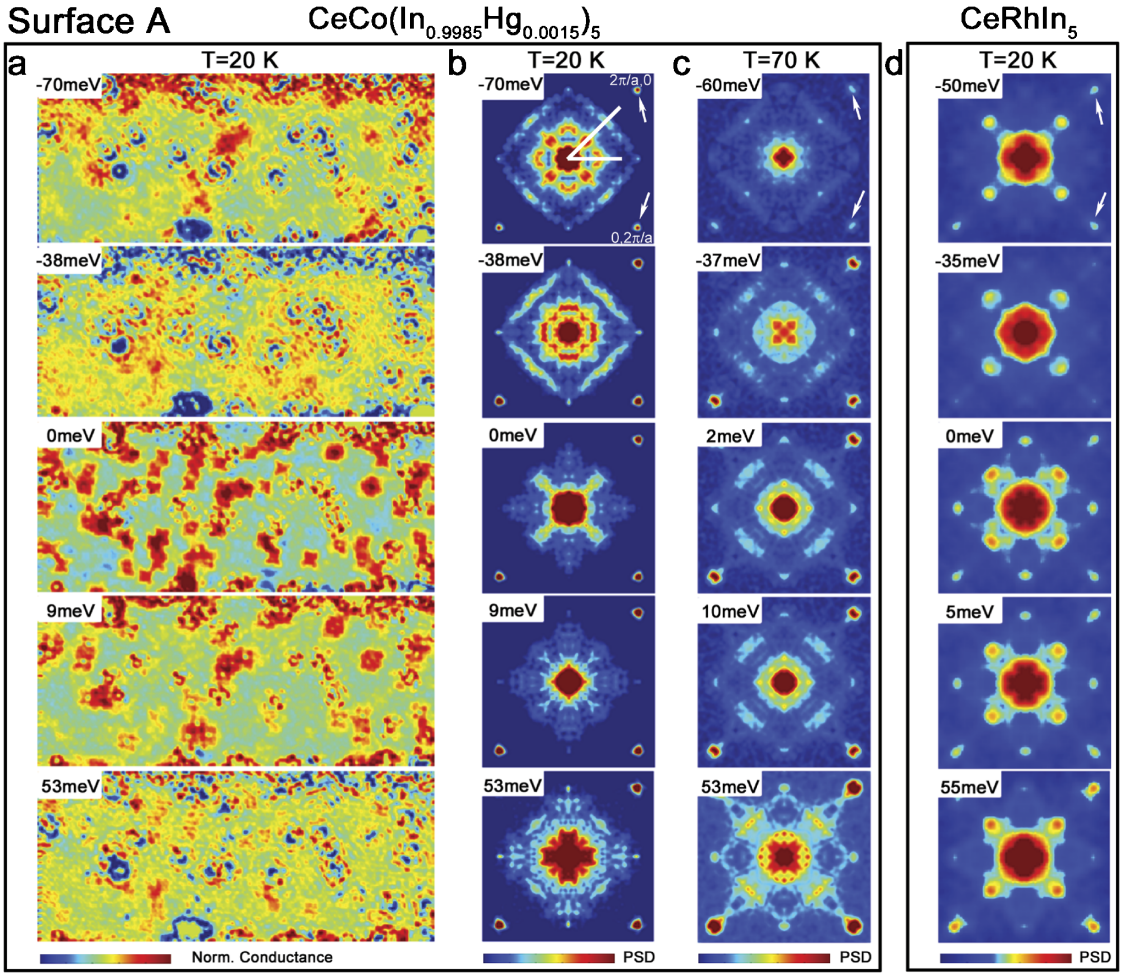

Fig. 5. (Color online) Spectroscopic mapping of quasiparticle interference on surface A. Real space (a) and corresponding DFT (b) of conductance maps (-200 mV, 1.6 nA) at selected energies measured on surface A of $CeCo(In_{0.9985}Hg_{0.0015})_5$ at 20 K. The sample was doped with 0.15% Hg to enhance scattering. This tiny impurity content does not change the thermodynamic behavior. Similar DFTs for $CeCoIn_5$ at 70 K (-150 mV, 1.5 nA) (c) and on the corresponding surface A for $CeRhIn_5$ at 20 K (-200 mV, 3.0 nA) (d) at selected energies. The arrow indicates the position of the Bragg peaks at $(2\pi/a, 0)$ and $(0, 2\pi/a)$. All DFTs were four-fold symmetrized (due to the four-fold crystal symmetry) to enhance the signal. The intensity is represented on a linear scale. Figure reproduced from Ref. 27.

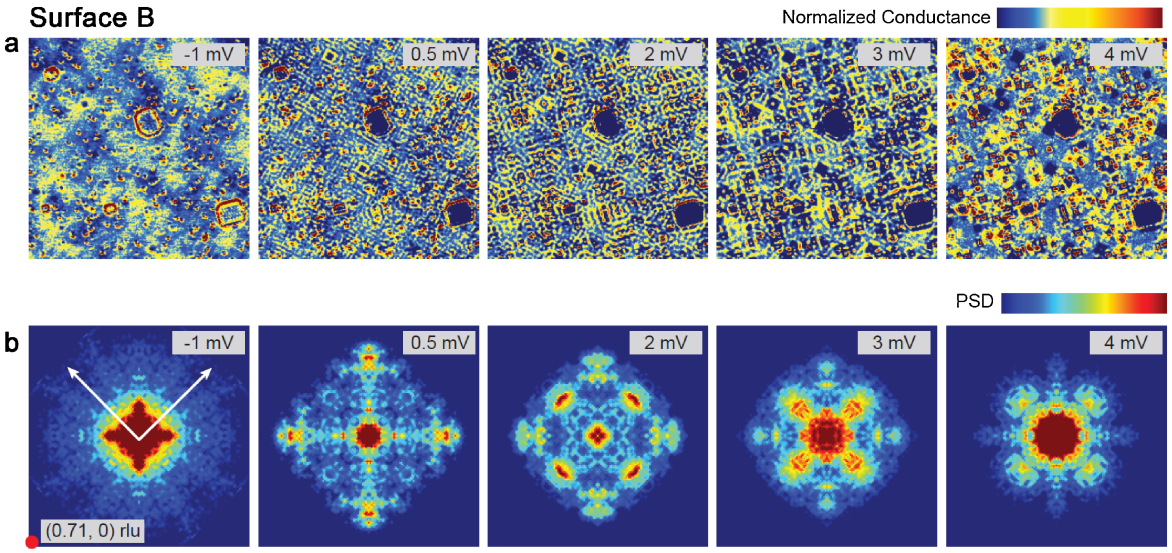

Fig. 6. (Color online) Spectroscopic mapping of quasiparticle interference on surface B. Real space conductance maps (a) and their DFTs (b) at selected biases measured at $T = 245$ mK on surface B. Colorbar in (a) denotes deviation from the mean. Axes in (b) denote the Bragg orientation for all DFTs. The corners of the DFTs in (b) are $(\pm 0.71, 0)2\pi/a$, $(0, \pm 0.71)2\pi/a$. Figure reproduced from Ref. 28.

are absent [e.g., Fig. 3(a)] in the same temperature window (20 K). Whereas these measurements on surface A display QPI patterns dominated by the lighter part of the composite heavy fermion bands that weaken near E_F at low temperatures, measurements on surface B of $CeCoIn_5$ show a strongly dispersing QPI signal that is present only near E_F, in unison with related signatures in the tunneling spectra (Fig. 6).

Understanding details of the QPI in Figs. 5 and 6 requires detailed modeling of the complex band structure of the 115 compounds, which from previous theoretical calculations, quantum oscillation, and angle resolved photoemission spectroscopy measurements is known to consist of multiple three-dimensional bands.[39,40] These previous measurements and calculations have also shown that the so called α and β bands are the most relevant near E_F. Our QPI measurements show features that are consistent with $2k_F$ scattering originating from the α and β bands. However, inferring a unique Fermi surface from STM measurements in a three-dimensional, multi-band material without making large number of assumptions is not possible. Regardless, analyzing the features of the energy-resolved DFT maps provide direct evidence for mass enhancement of quasiparticles. Figures 7(a) and 7(b) show line cuts of the DFT maps plotted along two high symmetry directions as a function of energy for surface A of $CeCoIn_5$ at 20 K. The square-like regions of enhanced quasiparticle scattering in Fig. 5(b) appear in the line cuts of Figs. 7(a) and 7(b) as energy-dependent bands of scattering, which become strongly energy dependent near the Fermi energy. Clearly the scattering of the quasiparticle excitations in the energy window near the direct hybridization gap have flatter energy-momentum structure as compared to those at energies away from the gap. This is best seen on surface B of $CeCoIn_5$ at low temperatures, where tunneling is more sensitive to the heavy excitations near the Fermi energy [Figs. 7(c) and 7(d)]. This is the direct signature of the quasiparticles acquiring heavy effective mass at low energies near the Fermi energy. Detailed analysis of the QPI bands estimates the mass enhancement near the Fermi energy to be about $20–30m_0$ [Figs. 7(c) and 7(d)], a value which is close to that seen in quantum oscillation studies of $CeCoIn_5$.[30,31]

Contrasting low temperature QPI patterns on $CeCoIn_5$ to measurements on the same compound at high temperatures [70 K, Figs. 7(e) and 7(f)], where the hybridization gap is weak, or to measurements on $CeRhIn_5$ [20 K, Figs. 7(g) and 7(h)], where signatures of a hybridization gap are absent in the tunneling spectra, confirms that the development of this gap results in apparent splitting of the bands which are responsible for both the scattering and the heavy effective mass in the QPI measurements. Furthermore, these measurements show that the underlying band structure responsible for the scattering wavevectors away from the Fermi energy is relatively similar between $CeCoIn_5$ and $CeRhIn_5$. Only when *f*-electrons of the Kondo lattice begin to strongly hybridize with conduction electrons and modify the band structure within a relatively narrow energy window (≈30 meV), we see signatures of heavy fermion excitations in QPI measurements, signaling a transition from small to large Fermi surface.

2.5 *Heavy electron superconductivity in CeCoIn$_5$*

We now turn to low temperatures to address the emergence

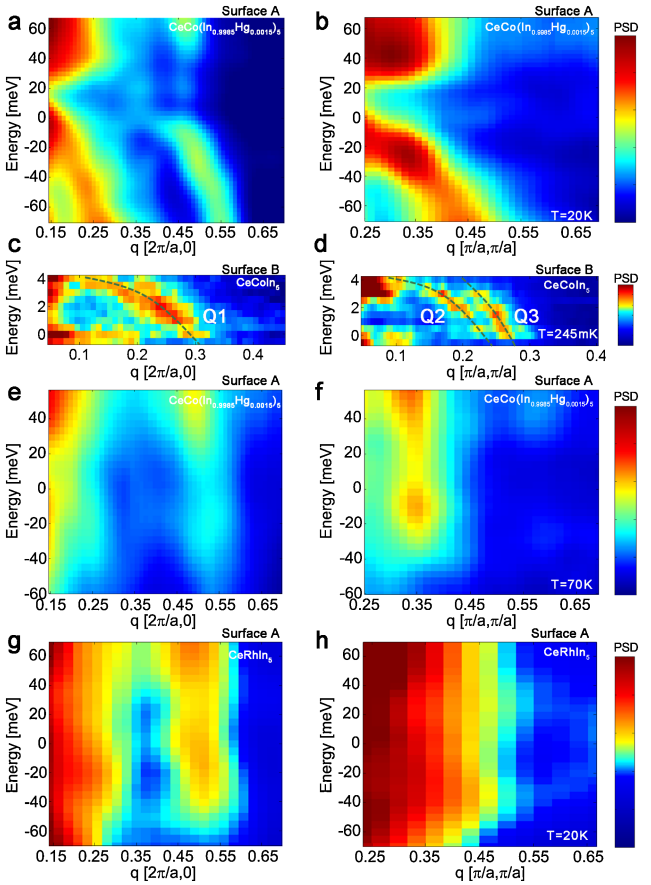

Fig. 7. (Color online) Visualizing quasiparticle mass enhancement. (a, b) Energy-momentum structure of the QPI bands on Surface A of $CeCo(In_{0.9985}Hg_{0.0015})_5$ at 20 K extracted from line cuts (solid white lines in Figs. 5 and 6) along the atomic direction $(2\pi/a, 0)$ (a) and along the zone diagonal $(\pi/a, \pi/a)$ (b). (c, d) Energy-momentum structure of the QPI bands on Surface B of $CeCoIn_5$ at 245 mK along the same two high symmetry directions. The effective mass $m^* = 34\,m_0$, $29\,m_0$, $23\,m_0$ for the three different bands (Q1, Q2, Q3) respectively is extracted from the curvature $(1/4\,\hbar^2[d^2E/dq^2]^{-1})$ of a second order polynomial fits to the QPI bands. Error bars are derived from the width of the peaks in the DFTs. (e, f) Similar measurements performed on surface A of $CeCo(In_{0.9985}Hg_{0.0015})_5$ at 70 K. (g, h) Similar measurements performed on surface A of $CeRhIn_5$ at 20 K. PSD, power spectral density. The intensity is represented on a linear scale. Figure reproduced from Refs. 27 and 28.

of superconductivity in $CeCoIn_5$. The results of our QPI measurements in $CeCoIn_5$ at low temperatures [Figs. 7(a)–7(f)] together with spectroscopic measurements [Figs. 3(a) and 3(b)] demonstrate that the superconducting instability occurs within a correlated heavy quasiparticle band with a large density of states at the Fermi energy. Lowering the temperature below T_c shows that the spectrum on surface A, which displays the indirect hybridization gap, is modified by the onset of an energy gap associated with superconductivity [Fig. 8(a)]. However, instead of focusing on measurements of surface A, where the tunneling is dominated by the lighter part of the composite band, we turn to measurements of surface B, which probes the narrow bands of heavy excitations resulting in the double peak structure near E_F. Lowering the temperature from 7.2 to 5.3 K, above T_c, we find that this peak is modified by the onset of a pseudogap-like feature at a smaller energy scale [Fig. 8(b)]. Further cooling shows the onset of a distinct superconducting gap below T_c inside the pseudogap. Measurements in a magnetic

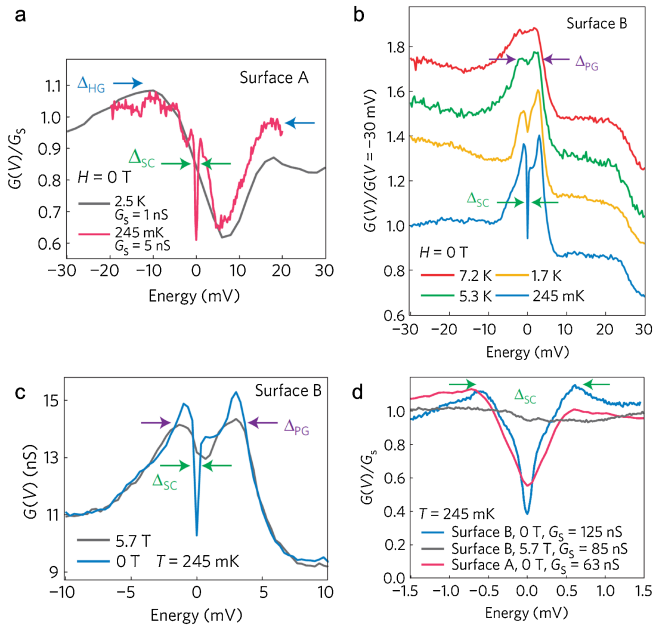

Fig. 8. (Color online) Hybridization, pseudogap, and superconductivity in $CeCoIn_5$. (a) Tunneling density of states on surface A carried out at temperatures above and below T_c. (b) Similar spectra on surface B of $CeCoIn_5$ showing the evolution of the different energy scales (Δ_{HG}: hybridization gap; Δ_{PG}: pseudogap; Δ_{SC}: superconducting gap) with temperature. Spectra are offset for clarity. (c) Blow up of the superconducting gap energy scale on surface B showing the destruction of the superconducting gap in a magnetic field of $H = 5.7\,\mathrm{T} > H_{c2}$ while the pseudogap feature is preserved. (d) Comparison of the superconducting energy scale on the two surfaces. The spectra $G(V)$ in (a) and (d) are normalized by their corresponding junction impedances G_S. Figure reproduced from Ref. 28.

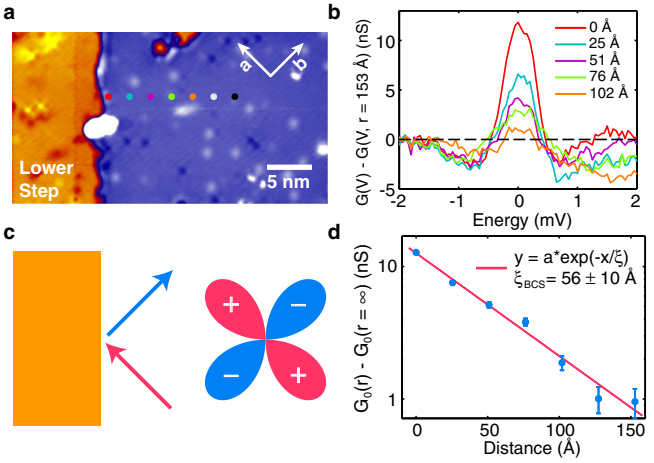

Fig. 9. (Color online) Evolution of in-gap quasiparticle states approaching a step-edge. (a) Topographic image ($V = -100\,\mathrm{mV}$, $I = 100\,\mathrm{pA}$) of surface A in $CeCoIn_5$ showing a single unit-cell step-edge oriented at 45° to the atomic lattice. The arrows in the figure indicate the in-plane crystallographic a- and b-directions. (b) Evolution of the spectra near the step-edge: $G(V)$ subtracted by the spectrum far away from the step-edge $G(V, r = 153\,\text{Å})$. The locations of the spectra in (b) are plotted on (a). (c) Schematic representation of nodal superconducting quasiparticles scattering off a step-edge. (d) Zero-bias conductance $G_0(r)$ subtracted by $G_0(r = \infty)$ as a function of distance from the step edge. Line represents an exponential fit to the data, where error bars denote the standard deviation on the averaged spectra. ξ_{BCS} denotes the characteristic decay length obtained from the fit in (d), which is a measure of the BCS coherence length. Figure reproduced from Ref. 28.

field corroborate our finding that the lowest energy scale on surface B [$\sim\pm500\,\mu\mathrm{V}$, as shown in Fig. 8(c)] is indeed associated with pairing, as it disappears above H_{C2}, while the intermediate energy scale pseudogap remains present at low temperature in the absence of superconductivity at high magnetic field [Fig. 8(c)]. This behavior is reminiscent of the pseudogap found in underdoped cuprates, where the superconducting gap opens inside an energy scale describing strong correlations that onset above T_c. However, unlike cuprates, here we clearly distinguish between the two energy scales by performing high-resolution spectroscopy in a magnetic field large enough to fully suppress superconductivity. The spectroscopic measurements suggest that electronic or magnetic correlations alter the spectrum of heavy excitations by producing a pseudogap within which pairing takes place. These measurements also show the shape of the spectra at the lowest temperature to be most consistent with a d-wave superconducting gap, as they have a nearly linear density of states near zero energy (Fig. 8). However, measurements on all surfaces and on several samples reveal that this d-wave gap (with a magnitude of $535 \pm 35\,\mu\mathrm{V}$, consistent with that extracted from point contact data[18,19]) is filled (40%) with low energy excitations — a feature that cannot be explained by simple thermal broadening (determined to be 245 mK). The complex multiband structure of $CeCoIn_5$ could involve different gaps on different Fermi surface sheets, and there is the possibility that some remain ungapped even at temperatures well below T_c.[41] Another contribution to the in-gap density of states could come from surface impurities, since even non-magnetic impurities perturb a nodal superconductor.

The first such signature can be found by examining the response of low-energy excitations to extended potential defects such as atomic step edges. Spectroscopic mapping with the STM upon approaching such steps shows direct evidence for the suppression of superconductivity in their immediate vicinity [Figs. 9(a) and 9(b)]. This suppression is consistent with the expected response of a nodal superconductor to non-magnetic scattering [Fig. 9(c)], analogous to similar observations in the cuprates,[42] and in marked contrast with step-edge measurements of conventional s-wave superconductors.[28] The data in Fig. 9(d) provide a direct measure of the Bardeen–Cooper–Schriefer (BCS) coherence length[43] $\xi_{BCS} = 56 \pm 10\,\text{Å}$, in agreement with $\xi_{BCS} \sim \hbar v_F/\pi\Delta \sim 60\,\text{Å}$ using the gap observed in Fig. 8 (0.5 meV) and the Fermi velocity extracted from Fig. 7 (1.5×10^6 cm/s).

A more spectacular demonstration of the nodal pairing character in $CeCoIn_5$ can be obtained from examining the spatial structure of in-gap states associated with defects on the surface of cleaved samples. The spatial structure of impurity quasi-bound states, which are mixtures of electron- and hole-like states, can be a direct probe of the order parameter symmetry. Figure 10 shows an extended defect with a four-fold symmetric structure, which perturbs the low energy excitations of $CeCoIn_5$ by inducing an in-gap state. Probing the spatial structure of these impurity states, we not only find their expected electron–hole asymmetry, but also find that their orientation is consistent with that predicted for a $d_{x^2-y^2}$ superconductor [Figs. 10(b)–10(e)].[32,44] The minima

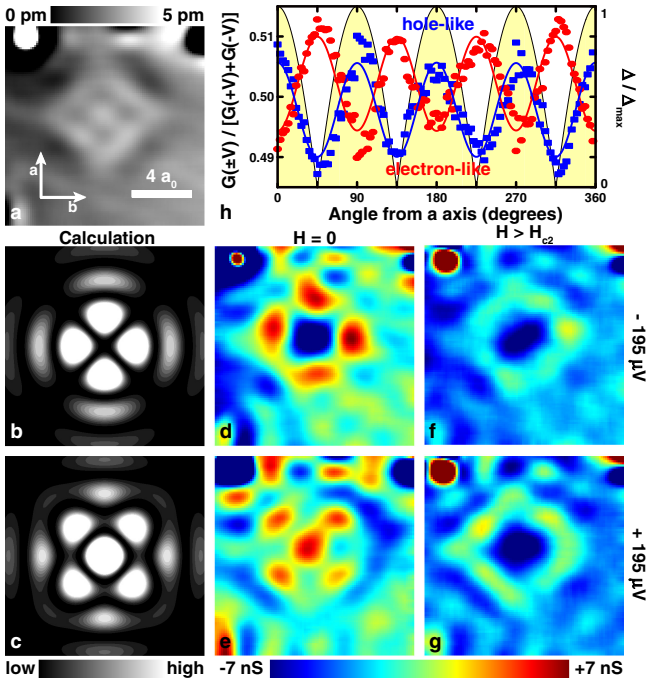

Fig. 10. (Color online) Visualizing impurity-bound quasiparticle excitations. (a) Topographic image of an impurity on surface B ($V = -6$ mV, $I = 100$ pA). (b) Model calculation for the real space structure (roughly 10 Fermi wavelengths across) of the hole-like part of the impurity bound state in a $d_{x^2-y^2}$ superconductor, reproduced from Ref. 44. (c) Electron-like state for the same impurity in (b). (d–g) Local density of states obtained on the same field-of-view as (a) at $\pm 195\,\mu$V in the normal ($H > H_{c2}$) and superconducting ($H = 0$) states as indicated on the figure. Colorbar in (d–g) denotes deviation from the mean. (h) Radial average of the density of states across the lobes measured in (d, e), normalized to their sum, as a function of angle from the b-axis. Data at negative (positive) energy is shown in blue (red) symbols; the lines are guides to the eye. A $d_{x^2-y^2}$ gap is shown in yellow. Figure reproduced from Ref. 28.

(maxima) in the oscillations for hole-like (electron-like) states identify the nodes of the d-wave order to occur at 45° to the atomic axes [Fig. 10(h)]. In fact, these features in the STM conductance maps are identical to those associated with Ni impurities in high-T_c cuprates.[43,45] However, in contrast to measurements in the cuprates, we are able to determine the spatial structure that such impurities induce on the normal state by suppressing pairing at high magnetic fields. Such measurements allow us to exclude the influences of the normal state band structure of the impurity shape, or of the tunneling matrix element[43] on the spatial symmetries of the impurity bound state in the superconducting state. Contrasting such measurements for $H > H_{C2}$ [in Figs. 10(f) and 10(g)] with measurements on the same impurity for $H = 0$ [Figs. 10(d) and 10(e)] we directly visualize how nodal superconductivity in $CeCoIn_5$ breaks the symmetry of the normal electronic states in the vicinity of a single atomic defect.

3. Conclusions

In summary, the experimental results and the model calculations presented here provide a comprehensive picture of how heavy fermion excitations in the 115 Ce-based Kondo lattice systems emerge with lowering of temperature or as a result of chemical tuning of the interaction between the Ce f-electrons and the conduction electrons. The changes in the scattering properties of the quasiparticles directly signal the flattening of their energy-momentum structure and the emergence of heavy quasiparticles near the Fermi energy. Such changes are also consistent with the predicted evolution from small to large Fermi surface as the localized f-electrons hybridize with the conduction electrons. The sensitivity of the tunneling to the surface termination and the successful modeling of these data provide direct spectroscopic evidence of the composite nature of heavy fermions and offer a unique method to disentangle their components. Spectroscopic signatures in $CeCoIn_5$ and URu_2Si_2 above T_{HO}, reveal a similar hybridization energy scale (30–40 meV), which mostly effects quasiparticles above the chemical potential. Furthermore, contrasting measurements above and below T_{HO}, show that the hidden order state in URu_2Si_2 opens a narrow gap near E_F with an energy scale much smaller than the hybridization gap. Finally, extending the measurements in $CeCoIn_5$ to very low temperatures reveals the appearance of a pseudogap and direct evidence for $d_{x^2-y^2}$ superconductivity, which ties the phenomenology of the Ce-115 system to that of the high-temperature cuprate superconductors.

Acknowledgements

We gratefully acknowledge discussions with P. W. Anderson, E. Abrahams, P. Coleman, N. Curro, D. Pines, D. Morr, T. Senthil, S. Sachdev, M. Vojta, and C. Varma. The work at Princeton was primarily supported by a grant from DOE-BES. The instrumentation and infrastructure at the Princeton Nanoscale Microscopy Laboratory used for this work were also supported by grants from NSF-DMR 1104612, the NSF-MRSEC program through Princeton Center for Complex Materials (DMR-0819860), the Wendy and Eric Schmidt Transformative Fund, and the W. M. Keck Foundation. P.A. acknowledges postdoctoral fellowship support through the Princeton Center for Complex Materials funded by the National Science Foundation MRSEC program. Work at Los Alamos was performed under the auspices of the U.S. Department of Energy, Office of Basic Energy Sciences, Division of Materials Science and Engineering. Z.F. acknowledges support from NSF-DMR-0801253.

*Present address: Department of Physics, Applied Physics and Astronomy, Binghamton University, Binghamton, NY 13902, U.S.A.
†Present address: Quantum Matter Institute, University of British Columbia, Vancouver, British Columbia V6T 1Z4, Canada.
‡yazdani@princeton.edu

1) G. Stewart, Rev. Mod. Phys. **56**, 755 (1984).
2) Z. Fisk, J. L. Sarrao, J. L. Smith, and J. D. Thompson, Proc. Natl. Acad. Sci. U.S.A. **92**, 6663 (1995).
3) A. Schröder, G. Aeppli, R. Coldea, M. Adams, O. Stockert, H. v. Löhneysen, E. Bucher, R. Ramazashvili, and P. Coleman, Nature **407**, 351 (2000).
4) P. Coleman, C. Pépin, Q. Si, and R. Ramazashvili, J. Phys.: Condens. Matter **13**, R723 (2001).
5) Q. Si, S. Rabello, K. Ingersent, and J. L. Smith, Nature **413**, 804 (2001).
6) T. Senthil, S. Sachdev, and M. Vojta, Phys. Rev. Lett. **90**, 216403 (2003).
7) T. Park, F. Ronning, H. Q. Yuan, M. B. Salamon, R. Movshovich, J. L. Sarrao, and J. D. Thompson, Nature **440**, 65 (2006).
8) P. Gegenwart, Q. Si, and F. Steglich, Nat. Phys. **4**, 186 (2008).
9) C. Pfleiderer, Rev. Mod. Phys. **81**, 1551 (2009).
10) T. T. M. Palstra, A. A. Menovsky, J. van den Berg, A. J. Dirkmaat, P. H. Kes, G. J. Nieuwenhuys, and J. A. Mydosh, Phys. Rev. Lett. **55**, 2727 (1985).

11) F. Steglich, C. Geibel, R. Modler, M. Lang, P. Hellmann, and P. Gegenwart, J. Low Temp. Phys. **99**, 267 (1995).
12) Y.-f. Yang, Z. Fisk, H.-O. Lee, J. D. Thompson, and D. Pines, Nature **454**, 611 (2008).
13) Q. Si and F. Steglich, Science **329**, 1161 (2010).
14) P. W. Anderson, Phys. Rev. Lett. **104**, 176403 (2010).
15) P. Coleman, *Handbook of Magnetism and Advanced Magnetic Materials* (Wiley, New York, 2007) Vol. 1.
16) C. Grenzebach, F. B. Anders, G. Czycholl, and T. Pruschke, Phys. Rev. B **74**, 195119 (2006).
17) J. H. Shim, K. Haule, and G. Kotliar, Science **318**, 1615 (2007).
18) L. C. Martin, M. Bercx, and F. F. Assaad, Phys. Rev. B **82**, 245105 (2010).
19) D. Jacob, K. Haule, and G. Kotliar, Phys. Rev. B **82**, 195115 (2010).
20) A. Benlagra, T. Pruschke, and M. Vojta, Phys. Rev. B **84**, 195141 (2011).
21) Y.-F. Yang, Phys. Rev. B **79**, 241107 (2009).
22) M. Maltseva, M. Dzero, and P. Coleman, Phys. Rev. Lett. **103**, 206402 (2009).
23) J. Figgins and D. K. Morr, Phys. Rev. Lett. **104**, 187202 (2010).
24) P. Wölfle, Y. Dubi, and A. V. Balatsky, Phys. Rev. Lett. **105**, 246401 (2010).
25) S. Sachdev, *Quantum Phase Transitions* (Cambridge University Press, Cambridge, U.K., 1999).
26) P. Aynajian, E. H. da Silva Neto, C. V. Parker, Y. Huang, A. Pasupathy, J. Mydosh, and A. Yazdani, Proc. Natl. Acad. Sci. U.S.A. **107**, 10383 (2010).
27) P. Aynajian, E. H. da Silva Neto, A. Gyenis, R. E. Baumbach, J. D. Thompson, Z. Fisk, E. D. Bauer, and A. Yazdani, Nature **486**, 201 (2012).
28) B. B. Zhou, S. Misra, E. H. da Silva Neto, P. Aynajian, R. E. Baumbach, J. D. Thompson, E. D. Bauer, and A. Yazdani, Nat. Phys. **9**, 474 (2013).
29) C. Petrovic, P. G. Pagliuso, M. F. Hundley, R. Movshovich, J. L. Sarrao, J. D. Thompson, Z. Fisk, and P. Monthoux, J. Phys.: Condens. Matter **13**, L337 (2001).
30) D. Hall, E. C. Palm, T. P. Murphy, S. W. Tozer, Z. Fisk, U. Alver, R. G. Goodrich, J. L. Sarrao, P. G. Pagliuso, and T. Ebihara, Phys. Rev. B **64**, 212508 (2001).
31) H. Shishido, R. Settai, S. Hashimoto, Y. Inada, and Y. Ōnuki, J. Magn. Magn. Mater. **272–276**, 225 (2004).
32) T. Timusk and B. Statt, Rep. Prog. Phys. **62**, 61 (1999).
33) C. Renner, B. Revaz, J. Y. Genoud, K. Kadowaki, and Ø. Fischer, Phys. Rev. Lett. **80**, 149 (1998).
34) E. G. Moshopoulou, J. L. Sarrao, P. G. Pagliuso, N. O. Moreno, J. D. Thompson, Z. Fisk, and R. M. Ibberson, Appl. Phys. A **74**, s895 (2002).
35) T. T. M. Palstra, A. A. Menovsky, and J. A. Mydosh, Phys. Rev. B **33**, 6527 (1986).
36) J. A. Mydosh and P. M. Oppeneer, Rev. Mod. Phys. **83**, 1301 (2011).
37) U. Fano, Phys. Rev. **124**, 1866 (1961).
38) M. Maltseva, M. Dzero, and P. Coleman, arXiv:0910.1138.
39) P. M. Oppeneer, S. Elgazzar, A. B. Shick, I. Opahle, J. Rusz, and R. Hayn, J. Magn. Magn. Mater. **310**, 1684 (2007).
40) R. Settai, H. Shishido, S. Ikeda, Y. Murakawa, M. Nakashima, D. Aoki, Y. Haga, H. Harima, and Y. Onuki, J. Phys.: Condens. Matter **13**, L627 (2001).
41) M. A. Tanatar, J. Paglione, S. Nakatsuji, D. G. Hawthorn, E. Boaknin, R. W. Hill, F. Ronning, M. Sutherland, L. Taillefer, C. Petrovic, P. C. Canfield, and Z. Fisk, Phys. Rev. Lett. **95**, 067002 (2005).
42) S. Misra, S. Oh, D. J. Hornbaker, T. DiLuccio, J. N. Eckstein, and A. Yazdani, Phys. Rev. B **66**, 100510 (2002).
43) A. V. Balatsky, I. Vekhter, and J.-X. Zhu, Rev. Mod. Phys. **78**, 373 (2006).
44) S. Haas and K. Maki, Phys. Rev. Lett. **85**, 2172 (2000).
45) E. W. Hudson, K. M. Lang, V. Madhavan, S. H. Pan, H. Eisaki, S. Uchida, and J. C. Davis, Nature **411**, 920 (2001).

Pegor Aynajian was born in Beirut, Lebanon. He received his Bachelor in Physics from the Lebanese University in Beirut (2003). He received his Masters degree in Physics from the University of Stuttgart (2005) and his Ph. D. from the Max Planck Institute for Solid State Research in conjunction with the University of Stuttgart (2009). He was a postdoctoral fellow at Princeton University (2009–2013). In 2013 he joined the Physics Department of Binghamton University as an Assistant Professor. His research interests are focused on strongly correlated electron systems with emphasis on heavy-electron materials and unconventional superconductivity using scanning tunneling spectroscopy and neutron/x-ray scattering.

Eduardo H. da Silva Neto was born in Recife, Brazil in 1985. He obtained his B.A. in Physics and Mathematics (2008) from Amherst College, and his M.S. (2010) and Ph. D. (2013) in Physics from Princeton University. Since 2013 he has been a Max-Planck-UBC postdoctoral research fellow for the Quantum Matter Institute at the University of British Columbia, and a Global Scholar at the Canadian Institute for Advanced Research (CIFAR), Quantum Materials program. His research has focused on the study of correlated electron systems, such as heavy-fermion materials and copper-oxide based superconductors, by the use of different spectroscopic techniques such as scanning tunneling microscopy, resonant x-ray scattering and angle-resolved photoemission.

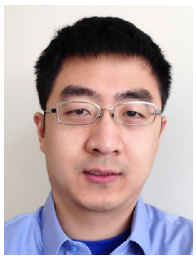

Brian B. Zhou was born in Hefei in Anhui Province, China in 1986. He obtained his B. Sc. (2008) from the California Institute of Technology and will obtain his Ph. D. (2014) from Princeton University. At Princeton (2008–2014), he worked to develop a dilution fridge-based, high magnetic field scanning tunneling microscope. His research focuses on probing superconductivity in strongly correlated electron systems, such as the heavy fermions and cuprates, and searching for novel electronic states in topological semi-metals.

Shashank Misra was born in Lucknow, India in 1977. He obtained his B.S. from the University of Wisconsin in 1998, and his Ph. D. from the University of Illinois at Urbana—Champaign in 2005. From 2005–2013, he worked as a postdoc, and then a lab manager, at Princeton University. During this time, his research interests varied from studying unconventional superconductors using scanning tunneling microscopy, to tunneling effects in bilayer quantum Hall systems, and the superfluid density near the superconductor-insulator transition in two dimensional thin films. He currently uses scanning tunneling microscopy to fabricate qubit devices in silicon at Sandia National Laboratories.

Zachary Fisk was born in New York in 1941. He obtained an AB from Harvard (1964) and a Ph. D. from UCSD (1969). He was a staff member at Los Alamos National Laboratory (1981–1994) and Professor of Physics at Florida State University and the NHMFL (1994–2004), UC San Diego (1992–1994), UC Davis (2004–2006) AND UC Irvine (2006 to present). His research has focussed on the heavy Fermion physics of $4f$ and $5f$ intermetallics using metallic flux growth for new materials search and crystal growth.

John A. Mydosh is professor emeritus of metal physics at the Kamerlingh Onnes Laboratory of Leiden University, The Netherlands. He has contributed to the physics of spin glasses, manganites, high-temperature superconductors and heavy-fermion materials.

Joe D. Thompson was born in Indiana U.S.A. in 1947. He obtained a B.S. degree from Purdue University (1969) and a Ph. D. from the University of Cincinnati (1975). He was postdoctoral scientist (1975–1977), staff member (1977–2001) and group leader (1992–2001) at Los Alamos National Laboratory and has been a Laboratory Fellow since 2001. His research has focused on new physics through new materials, with an emphasis on correlated electron materials at low temperatures, high pressures and high magnetic fields.

Eric D. Bauer received a B.S. in physics in 1996 from the University of California, Santa Cruz. He received a Ph. D. in physics from the University of California, San Diego in 2002. He was a Director's Funded Postdoctoral Fellow from 2002–2004, a Seaborg Postdoctoral Fellow from 2004–2005, and a Frederick Reines Distinguished Postdoctoral Fellow from 2005–2007 at Los Alamos National Laboratory, after which he became a member of the technical staff. In 2009, he received the Presidential Early Career Award for Scientists and Engineers (PECASE). His research interests include the synthesis of novel strongly correlated *f*- and *d*-electron materials, investigation of the localized/itinerant crossover in the actinides, unconventional superconductivity, and quantum criticality.

Ali Yazdani is a professor of Physics at Princeton University whose research program focuses on the development and application of novel experimental methods to directly visualize exotic electronic phenomena in solids. Yazdani received his BA in Physics from UC Berkeley in 1989, and his Ph. D. in Physics from Stanford University in 1995. He was a postdoctoral scientist at IBM's Almaden Research Center in California, where he pioneered experiments to probe superconductivity on the atomic scale with the scanning tunneling microscope in the early 90s. After IBM, he went on to establish a research program as a faculty member at the University of Illinois at Urbana — Champaign in 1997, and then as a professor of Physics at Princeton University in 2005. Yazdani's research program spans experiments on high temperature superconductivity, magnetism in semiconductors, nanoscience, and the newly discovered topological phases of electrons. Yazdani is a fellow of the American Association for Advancement of Science and American Physical Society.